

The Danish 1.54-m telescope on La Silla and the NEOSource project

Petr Pravec

Astronomical Institute AS CR, Ondřejov, Czech Republic

*Seminar „7 years in Chile: The Accomplishments and Goals of
Czech Astronomers at ESO“, Prague, 2014 April 14*

Contents

1. The Danish 1.54-m telescope, collaborative use and remote observations
2. The NEOSource project

The Danish 1.54-m telescope

A dedicated photometric telescope.

Owner: Niels Bohr Institute (NBI), Copenhagen University

Operated collaboratively by the NBI and the AI AS CR (plus the groups from MFF UK and PŘF MU) – The present agreement is for October 2012 to September 2018.



The Danish 1.54-m telescope

In 2012 the telescope was refurbished and a new control system was installed.

The author of the new control system is ProjectSoft HK.

The telescope upgrade was funded by the Academy of Sciences of the Czech Republic (with contributions from PřF MU Brno and MFF UK Prague) for our major project of studies of near-Earth asteroid properties, and for the supplementary projects of stellar photometry in support of Gaia and of Magellanic Clouds.



The Danish 1.54-m telescope

The telescope is fully remotely controlled – observations are done from our workplace here, no need for a local observer or technician at night.

ESO provides a few things: Electricity, daily LN2 refilling, internet connection.

We pay nightly fee to ESO for their service. Occasional technical interventions (typically one per 1-2 months) are paid per work person-hours.



DK154 parameters and capabilities

DFOSC + CCD camera in the
Cassegrain focus:

2k*2k, pixel scale 0.40", FOV 13'

Filters (in active use):

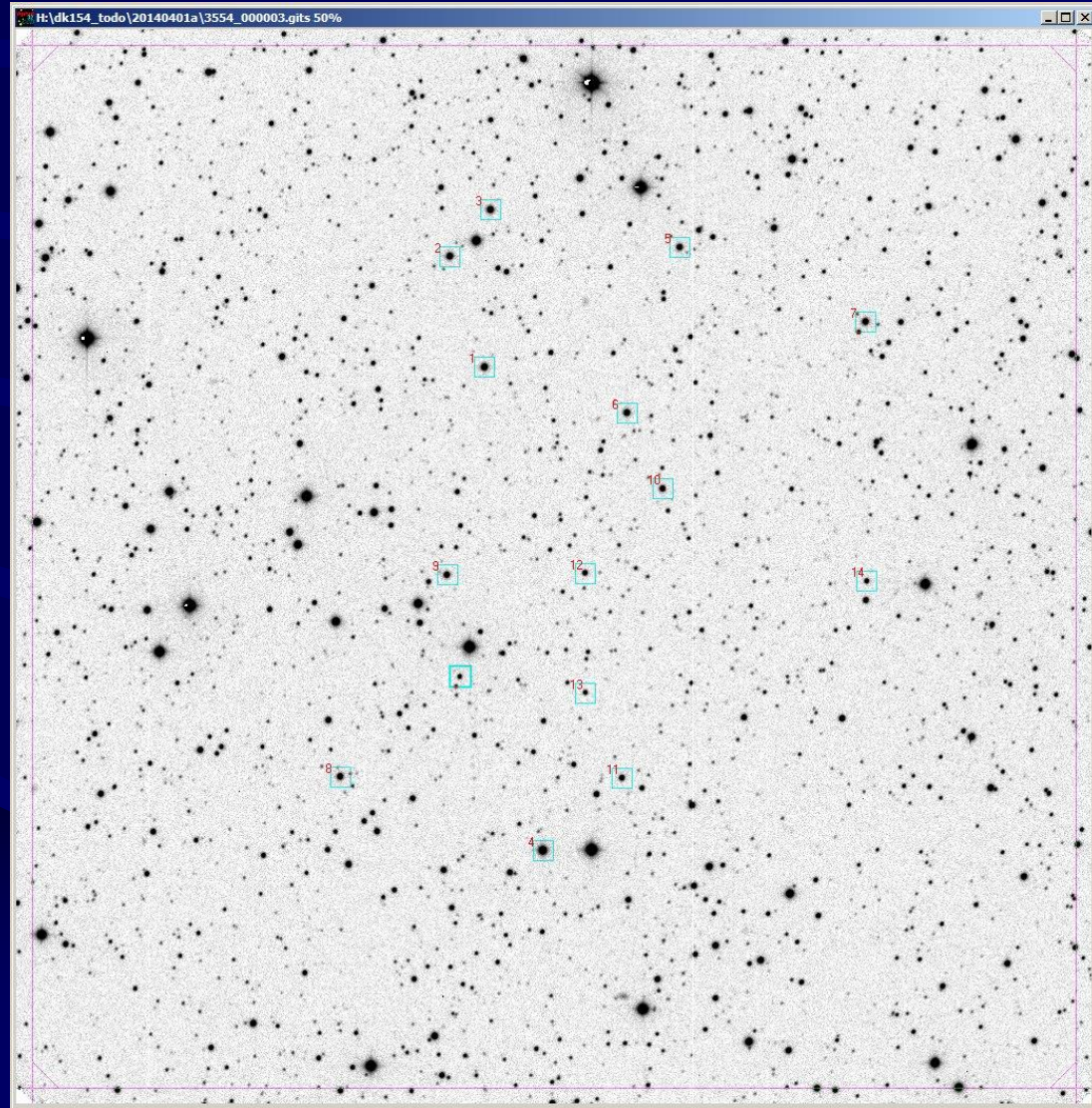
Johnson-Cousins (Bessell) UBVRI,
Stromgren ubvy, g2, Gunn z, H β .

Gain: 0.25 e⁻/ADU.

Dynamical range 19.4 bit (linearity
to 700 kADU).

Readout noise 4.5 e⁻

Full CCD readout time: 22 seconds.



DK154 parameters and capabilities

Limiting magnitude (3-min integration):

$$V_{\text{lim}} = 18.5 \text{ at SNR} = 100$$

$$V_{\text{lim}} = 20.0 \text{ at SNR} = 30$$

Typical seeing: <1" (median 0.8-0.9").

Fraction of usable night time (during our season October-April):

- Only 4% of nights have been totally lost due to bad weather.
- The net time loss has been 10% for weather and 4% for technical and other reasons.

DK154 control system

Highly automated operation.

Safety system – takes care of the telescope and dome in a case of

- bad weather
- human intrusion to the dome
- loss of remote observer's connection

The core is based on industrial components and solutions.

Many things are backed up, doubled (some even tripled), to eliminate as many bottle necks as possible.

Not robotic (yet).

Some things are script-controlled (under development).

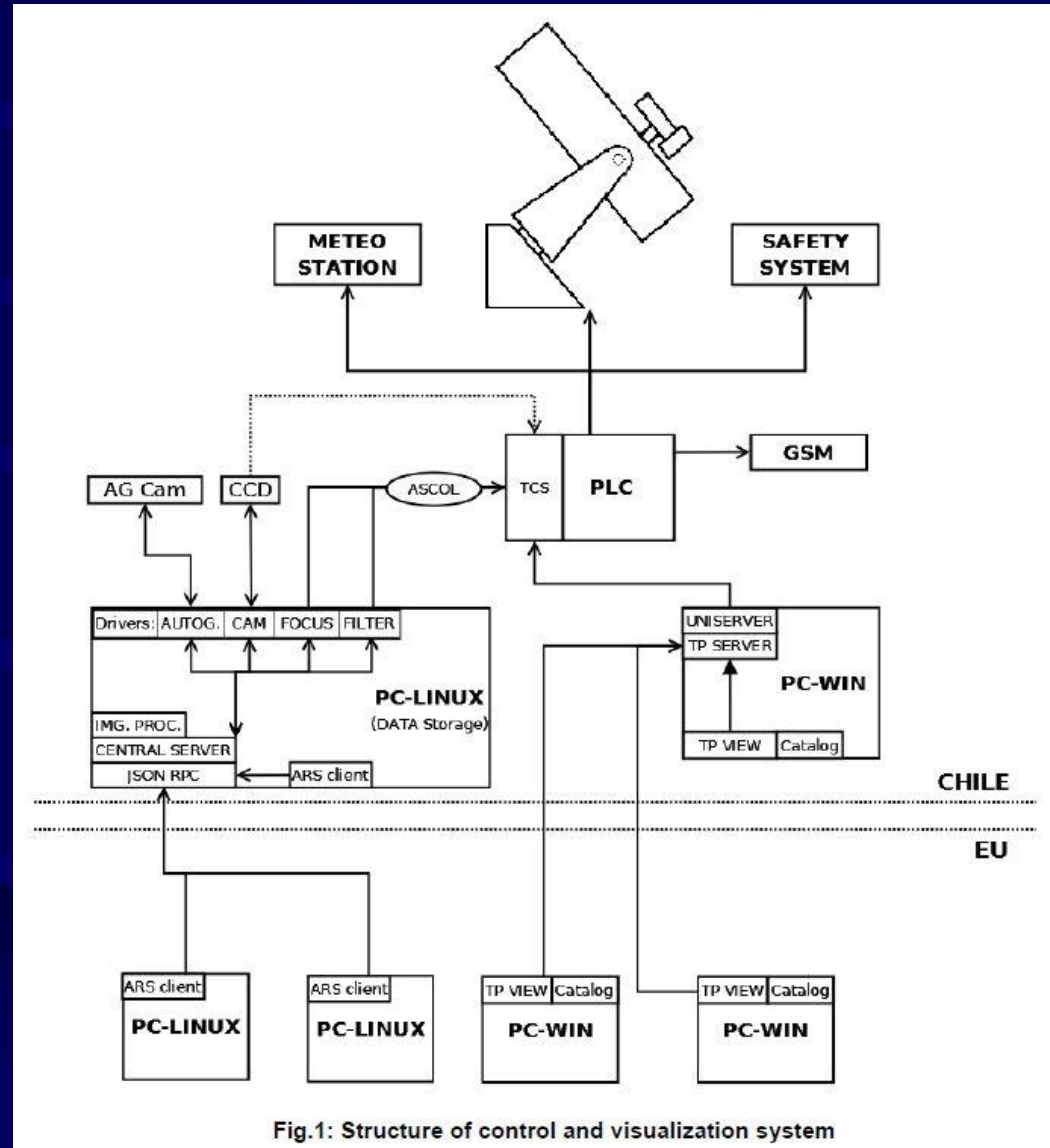


Fig.1: Structure of control and visualization system

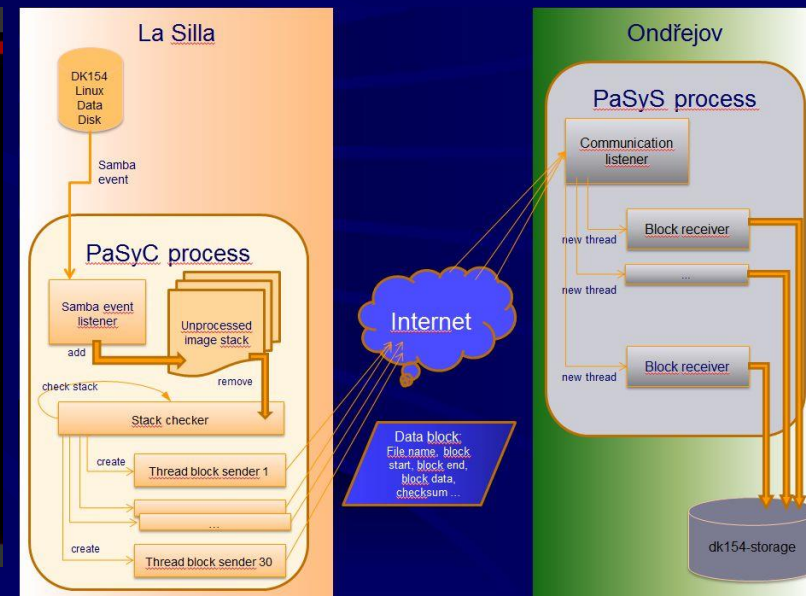
DK154 remote observations

Observer connects to the telescope via ESO_Santiago_VPN.

The Telescope Control System (TCS) and image acquisition clients run on local computer here and they communicate with the TCS server over the internet.

Images obtained are transferred to our dk154-data storage server in Ondřejov in near-real time (typically in 30 seconds after completing readout).

Direct connection and control is hampered/prohibited – there is the latency between La Silla and Europe (300 ms) that limits a use of non-parallelized communication.



DK154 remote observations

Observations partly automated

- automated image series acquisition
- automated focusing, autoguiding
- scripting (under development) – automatic field sequencing, flat field frames acquisition

Not really robotic:
Observer cannot sleep
(at least not for a longer
time ☺).

The screenshot shows the 'Astro Robotic System' control window. It includes a menu bar (File, Edit, Help), a status bar with local and server times, and a connection status. Below this are tabs for ARS, Focusing, Camera, A. Guider, and Log. A 'Select camera' dropdown is set to 'Main Camera'. The 'Current state' section shows 'Auto Focusing: IDLE' with 'Steps to end: 0' and 'Focuser status: IDLE' with 'Current position: 38.182'. A 'Setting' button is present. A graph plots focus position over time, showing a parabolic curve. At the bottom, there are 'Commands' for setting position and buttons for 'Focus' and 'Stop'.

The 'Camera setting' window displays 'Auto Guiding: AUTOGUIDING'. It features three sub-plots: 'Pointing win.' showing a star field, 'Sum of rows' showing a peak in the row sum, and 'Sum of columns' showing a peak in the column sum. Below these is a 'Star searching' window with a large image of a star field and a green crosshair. At the bottom, two graphs show 'RA deviation' and 'DEC deviation' over time, both exhibiting a sawtooth pattern.

The 'dk154_batch.py' window shows a table of observation parameters. The table has columns for Field, FilterB, Exptime, Count, Telpos, RA, DEC, Delay, FilterA, Focus, and Enable. The data is as follows:

Field	FilterB	Exptime	Count	Telpos	RA	DEC	Delay	FilterA	Focus	Enable
86039_320	R	18	1	M	064539.00	132325.00	0	empty	0	<input checked="" type="checkbox"/>
86039_402a	R	18	1	M	080112.00	095200.00	0	empty	0	<input checked="" type="checkbox"/>
86039_402b	R	18	1	M	080215.00	094900.00	0	empty	0	<input checked="" type="checkbox"/>
86039_403	R	18	1	M	080604.00	093625.00	0	empty	0	<input checked="" type="checkbox"/>
E101	R	15	3	M	095730.00	-002000.00	0	empty	0	<input checked="" type="checkbox"/>
E101	V	15	3	M	095730.00	-002000.00	0	empty	0	<input checked="" type="checkbox"/>
86039_320	R	15	4	M	064539.00	132325.00	0	empty	0	<input checked="" type="checkbox"/>
86039_403	V	15	4	M	080604.00	093625.00	0	empty	0	<input checked="" type="checkbox"/>
E101	V	15	3	M	095730.00	-002000.00	0	empty	0	<input checked="" type="checkbox"/>
E101	R	15	3	M	095730.00	-002000.00	0	empty	0	<input checked="" type="checkbox"/>
21436_222	R	40	1	M	104737.00	051718.00	0	empty	0	<input checked="" type="checkbox"/>
21436_402	R	40	1	M	101601.00	070610.00	0	empty	0	<input checked="" type="checkbox"/>

At the bottom of the window, there are settings for 'Auto stop' (00:00), 'Count repeat' (1), and 'Default focus absolute position' (39.00 mm). There are also checkboxes for 'Pointing restrictions' and 'enabled' for the auto stop and focus settings. Buttons for 'Start', 'Stop', 'Open file', 'Reload file', and 'Load from schedules' are at the bottom.

Science projects running at DK154

Danish, Czech, and Chilean time

DK154 collaborative use

Danish season, 6 months from mid-April to mid-October (minus 10% given to Chileans)

Main project:

MiNDSTeP (Microlensing Network for the Detection of Small Terrestrial Exoplanets)

www.mindstep-science.org

Czech season, the other 6 months (minus 10% given to Chileans)

NEOSource (PI P. Pravec, Co-PI D. Vokrouhlický) – 82 nights per year

Gaia Support (PI P. Koubský)

LSMC Prague (PI M. Wolf)

LSMC Brno (PI M. Zejda)

- 27 nights/year each.

Chilean observations

ESO's contractual obligations to the Chilean astronomy: 10% of nights offered to Chileans, i.e., 36 nights/year.

They mostly observe transits of exoplanets.

Evening Date	Scheduled		Observed			Time Lost (%)			Remark
	Program	Observer	Program	Supplementary	Observer(s)	Weather	Tech	Other	
5.10.13 Sat									
6.10.13 Sun									
7.10.13 Mon									
8.10.13 Tue									
9.10.13 Wed									
10.10.13 Thu									
Danish season									
11.10.13 Fri	NEOSource	Ku+KH	NEOSource		Ku+KH	0			8870 + 101703 + 8306
12.10.13 Sat	NEOSource	Ku+KH	NEOSource		Ku+KH	0			8870 + 101703 + 8306
13.10.13 Sun	LSMCPrague	PZ	LSMCPrague		PZ	0			
14.10.13 Mon	LSMCPrague	PZ	LSMCPrague		MW+LP	70			
15.10.13 Tue	LSMCPrague	PZ	LSMCPrague		PZ+KH	0			
16.10.13 Wed	LSMCBrno	MS	LSMCBrno		MS+KH	0			
17.10.13 Thu	LSMCPrague	JV	LSMCPrague		JV+KH	0			
18.10.13 Fri	LSMCPrague	JV	LSMCPrague		JV+KH	2			
19.10.13 Sat	GaiaSupp	JB	GaiaSupp		JB+KH	0			
20.10.13 Sun	GaiaSupp	JB	GaiaSupp		JB+KH	0			
21.10.13 Mon	GaiaSupp	JB				100			
22.10.13 Tue	LSMCBrno	MS				100			
23.10.13 Wed	LSMCBrno	JJ	LSMCBrno		JJ	21			
24.10.13 Thu	NEOSource	KH+PP	NEOSource		KH+PP+JV	3			101703 + 88710 + 8306
25.10.13 Fri	NEOSource	KH+PP	NEOSource		KH+JV+PP	0			101703 + 57738 + 88710 + 8306
26.10.13 Sat	NEOSource	KH+PP	NEOSource		KH+JV+PP	0			101703 + 57738 + 53537 + 8306
27.10.13 Sun	NEOSource	KH+PP	NEOSource		KH+JV+PP	0			101703 + 57738 + 76148 + 8306
28.10.13 Mon	NEOSource	KH+PP	NEOSource	LSMCBrno	KH+JV+PP+JV	19			53537 + 8306
29.10.13 Tue	NEOSource	KH+PP+Ku	NEOSource		KH+JV+PP+Ku+AG	22			53537 + 215619 + 8306 (event)
30.10.13 Wed	NEOSource	Ku+AG	NEOSource		Ku+AG	12			53537 + 215619 + 8306 + 138852
31.10.13 Thu	NEOSource	Ku+AG	NEOSource		AG	88			8306
1.11.13 Fri	LSMCPrague	PZ	LSMCPrague		PZ	70			
2.11.13 Sat	LSMCBrno	MZ+	LSMCBrno		MZ+JL	0			
3.11.13 Sun	LSMCBrno	MZ+	LSMCBrno		MZ+JL	0			
4.11.13 Mon	NEOSource	Ku+AG	NEOSource		AG+Ku	0			57738 + 138852 + 8306 (event)
5.11.13 Tue	NEOSource	Ku+AG	NEOSource		AG+Ku	0			215619 + 138852 + 8306
6.11.13 Wed	NEOSource	Ku+AG	NEOSource		AG+Ku	0			215619 + 138852 + 8306 + 53537
7.11.13 Thu	NEOSource	KH+Ku+AG	NEOSource		AG+KH+Ku	0			215619 + 138852 + 8306 (event) + 53537
8.11.13 Fri	NEOSource	Ku+AG	NEOSource		Ku+AG	0			215619 + 138852 + 8306 + 53537
9.11.13 Sat	NEOSource	Ku+AG	NEOSource		Ku+AG	72			76148 + 53537
10.11.13 Sun	NEOSource	KH+Ku	NEOSource		KH+Ku	13			76148 + 53537 + 138852
11.11.13 Mon	LSMCPrague	PZ+JV	LSMCPrague		JV+MW	0			
12.11.13 Tue	LSMCPrague	PZ+JV	LSMCPrague		PZ	0			
13.11.13 Wed	GaiaSupp	PS	GaiaSupp		LR+LK+EK	0			
14.11.13 Thu	GaiaSupp	PS	GaiaSupp		PS	0			
15.11.13 Fri	GaiaSun	PR	GaiaSun		SR+VV	0			

NEOSource project

Study of non-gravitational asteroid evolution processes via photometric observations

NEOSource project

Study of non-gravitational asteroid evolution processes via photometric observations
PI Petr Pravec, Co-PI David Vokrouhlický
Supported by GAČR, grant P209/12/0229.

2012 October – 2016 December, observations on 82 nights/year with the 1.54-m telescope at La Silla.

The effects we study can be detected with long-term monitoring, hence the need of a dedicated telescope.

A look ahead:

Recently we have submitted a proposal to the EC Horizon 2020-PROTEC-2-NEOs call. We have formed a consortium of NEO research groups from 10+ European countries, called *The European NEO Science Network*. The project will run during 2015-2018. Will provide a deep understanding of NEO properties using several observational techniques and extensive modeling. Will also characterize NEO targets for spacecraft missions, both human and robotic.

NEOSource project - Tasks

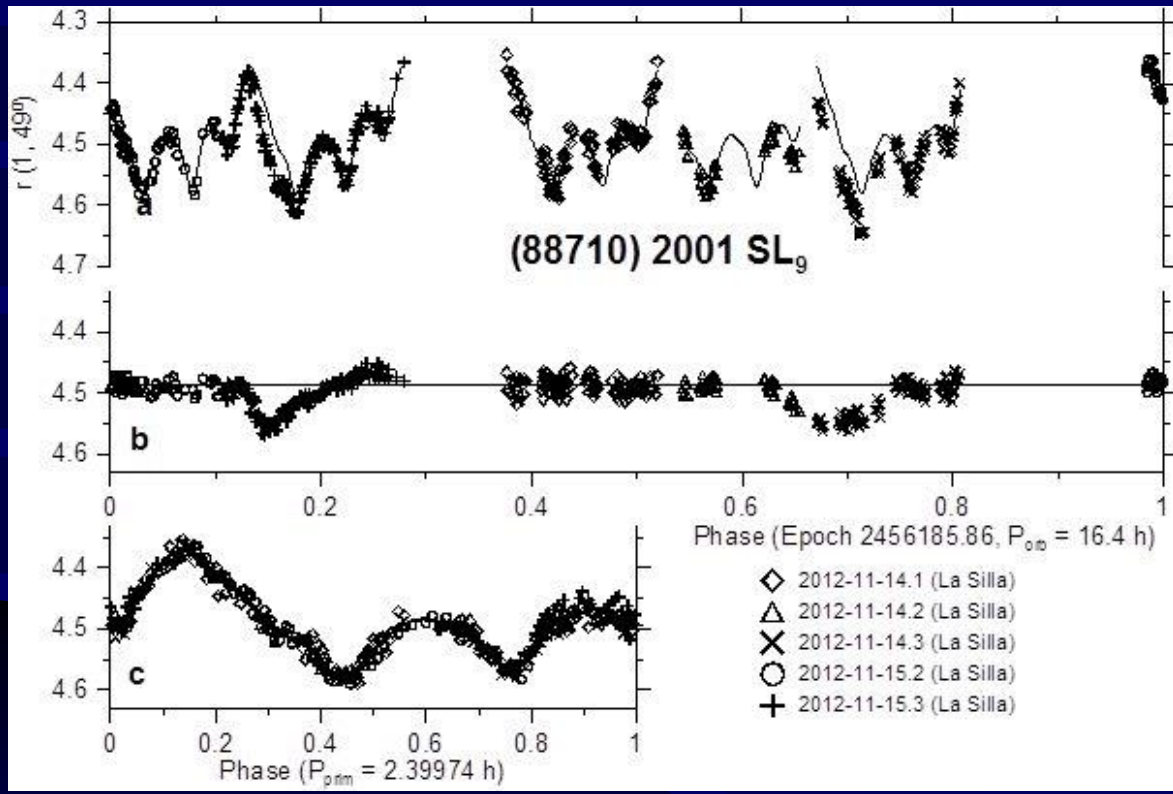
1. BYORP effect in near-Earth binary asteroids
2. Multiplicity of asteroid pairs
3. Spin vectors of asteroid pairs
4. Size ratios of asteroid pairs with small nominal astrometric dH
5. YORP effect in NEAs, enlarging the sample
6. Spin vectors in the Datura collisional family
7. Survey for tumblers among super-fast rotating NEAs
8. Spins of the largest members of asteroid clusters/mini-families
9. Spin rates and vectors of asteroids with detected Yarkovsky effect

Binary systems among NEAs and small MBAs

Improving their understanding (Task 1,
detection of the BYORP effect)
and relation with other asteroidal phenomena
(Task 2, multiplicity of paired asteroids)

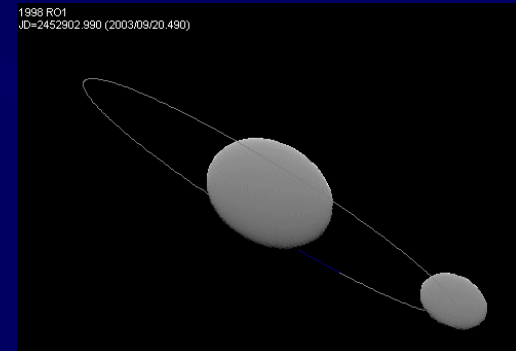
Binary near-Earth asteroid (88710) 2001 SL9

- candidate for BYORP effect detection (Task 1)

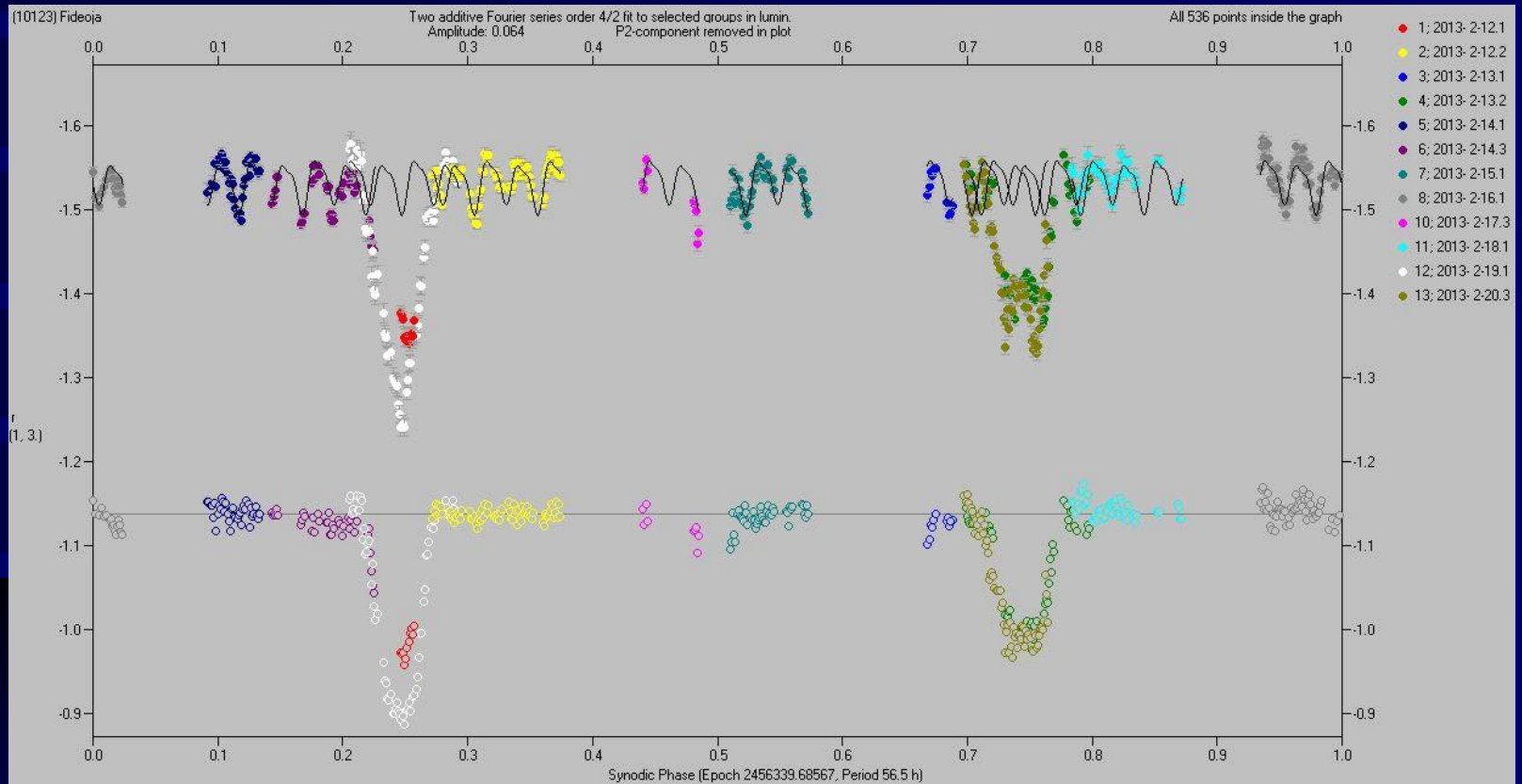


Photometric errors
0.013 mag

Derivable parameters: P_1 , P_{orb} , (P_2), D_2/D_1 , a_1/b_1 , (a_2/b_2)
and finally (with long-arc observations) L_p , B_p , e



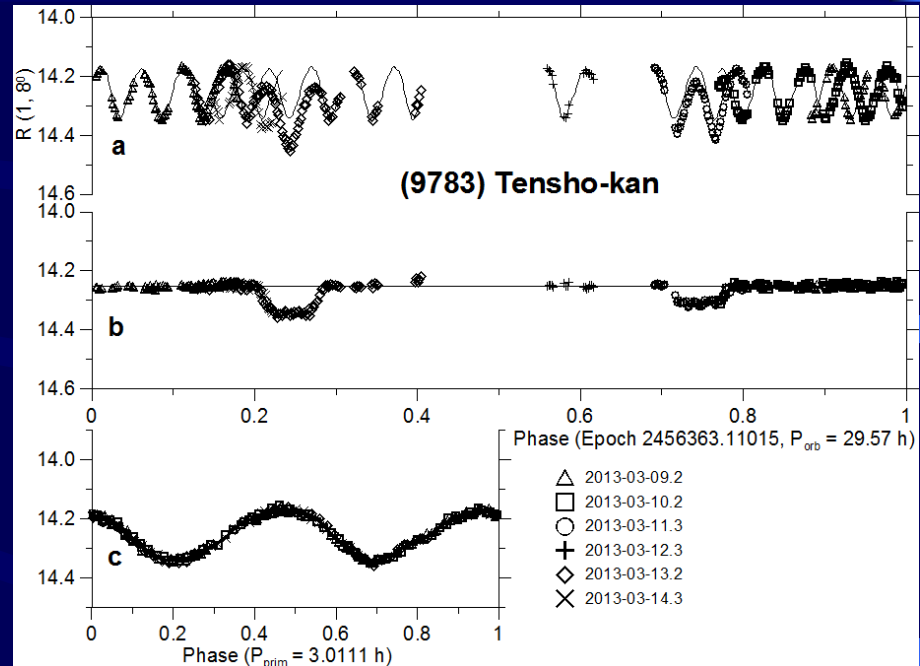
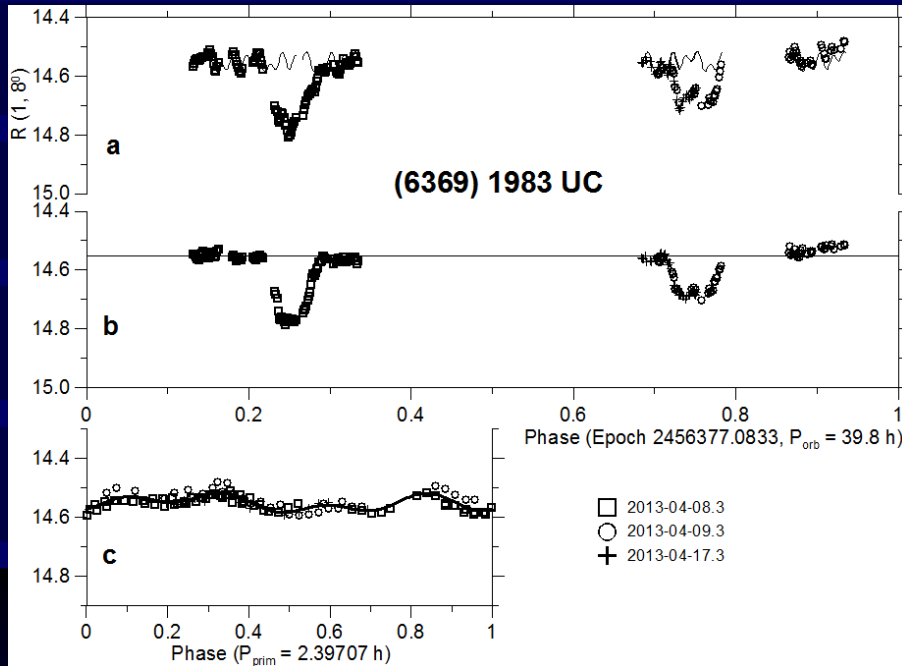
Binary paired asteroid (10123) Fideoja (Task 2)



$$P_{orb} = 56.5 \pm 0.1 \text{ h}$$
$$P_1 = 2.8658 \pm 0.0003 \text{ h}$$
$$D_2/D_1 = 0.39 \pm 0.02$$

Photometric errors
0.011 mag

Paired binaries (6369) and (9783)



They look pretty much like classical (semi-)asynchronous binaries ---except for their relatively long orbital periods--- with near-critical total angular momentum and nearly-spheroidal primary.

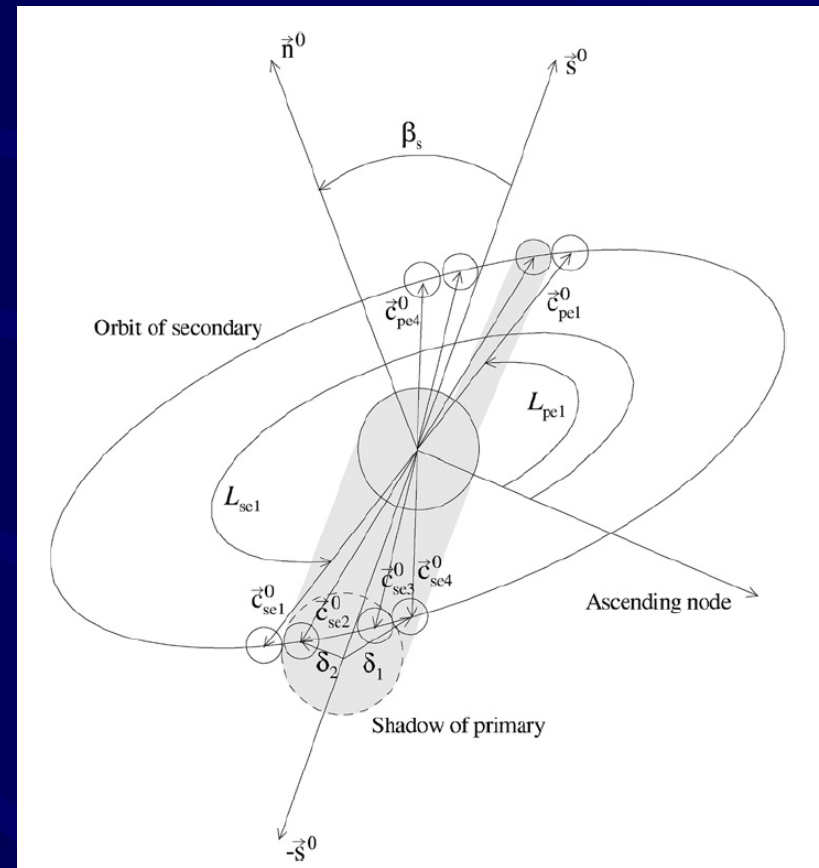
But we'll look forward towards seeing more data from their return apparitions.

Photometric detection of binary system - principle

Mutual occultation/eclipse events
between system components cause
brightness attenuations.

Condition:
Earth or Sun close to the system's orbit
plane.

Primary and secondary events
(depending on which body is
occulted/eclipsed).



(Scheirich and Pravec 2009)

Asteroid pairs among small MBAs

Related to orbiting bound binaries – formation
by rotational fission
(Tasks 2, 3 and 4)

Asteroid Itokawa

Can it fission when spun up?

BODY

HEAD

Release 051101-1 ISAS/JAXA

図3 イトカワの +90 度面



Asteroid pairs found on closely similar heliocentric orbits

Vokrouhlický and Nesvorný (Astron. J. 136, 280, 2008; VN08) found a population of pairs of asteroids residing on closely similar orbits.

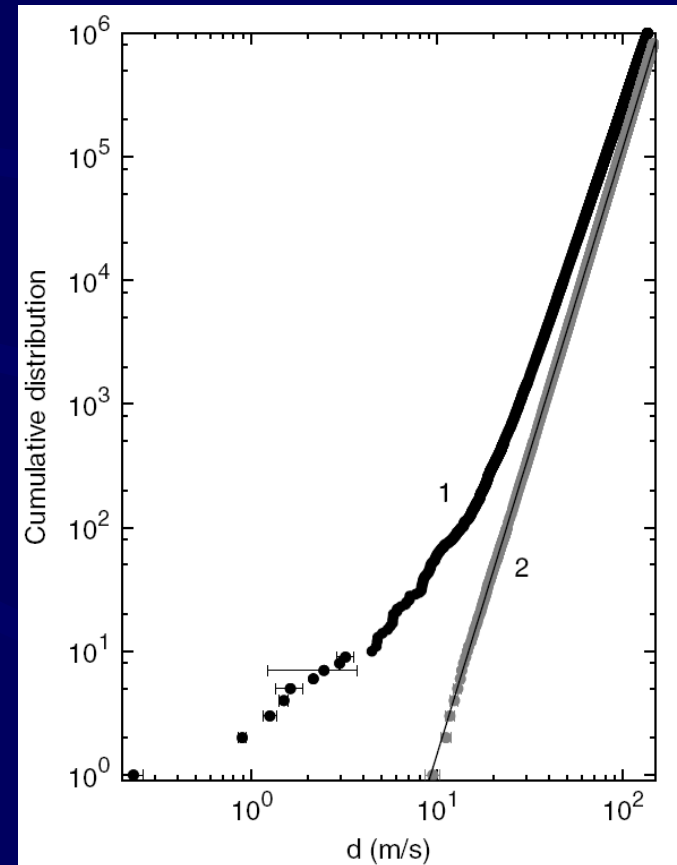
Pravec and Vokrouhlický (Icarus 204, 580, 2009; PV09) extended the analysis and found numerous significant pairs up to $d = 36$ m/s (approx. the current relative encounter velocity between orbits).

d in 5-dimensional space of osculating orbital elements $(a, e, i, \varpi, \Omega)$ defined as a positive-definite quadratic form:

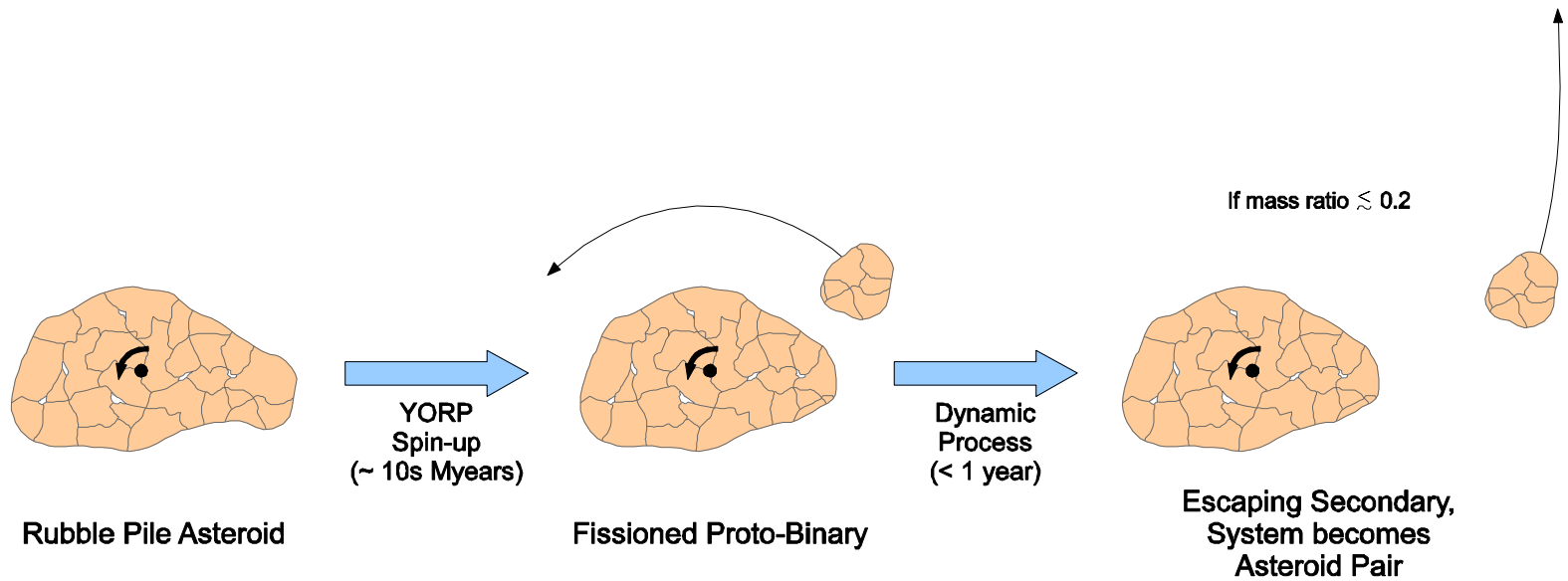
$$\left(\frac{d}{na}\right)^2 = k_a \left(\frac{\delta a}{a}\right)^2 + k_e (\delta e)^2 + k_i (\delta \sin i)^2 + k_\Omega (\delta \Omega)^2 + k_\varpi (\delta \varpi)^2, \quad (1)$$

where n and a is the mean motion and semimajor axis of either of the two asteroids and $(\delta a, \delta e, \delta \sin i, \delta \varpi, \delta \Omega)$ is the separation vector of their orbital elements.¹

	a	e	i	Omega	omega
4765	1.9455258	0.0604289	23.70505	76.59085	108.05341
2001X0105	1.9455837	0.0604382	23.70634	76.52980	108.30700
	-0.0000578	-0.0000093	-0.00129	0.06105	-0.25359



Pair formation by spin fission due to YORP spin-up



Rotational fission theory (Scheeres 2007, Pravec et al. 2010): Spun-up by YORP, the “rubble pile” asteroid reaches a critical spin rate and fissions. The secondary orbiting the primary, energy being transferred from rotational to translational energy and vice-versa. If $q < \sim 0.2$, the proto-binary has a positive free energy and the two components can escape from each other, after a period of chaotic orbit evolution (~ several months), and become an “asteroid pair”.

The total angular momentum and energy are, in general, conserved across fission but becomes decomposed into multiple components:

$$\mathbf{I} \cdot \boldsymbol{\omega} = \mathbf{I}_1 \cdot \boldsymbol{\omega}_1 + \mathbf{I}_2 \cdot \boldsymbol{\omega}_2 + \frac{M_1 M_2}{M_1 + M_2} \mathbf{r} \times \mathbf{v} \quad (7)$$

$$\frac{1}{2} \boldsymbol{\omega} \cdot \mathbf{I} \cdot \boldsymbol{\omega} + \mathcal{U} = \frac{1}{2} \boldsymbol{\omega}_1 \cdot \mathbf{I}_1 \cdot \boldsymbol{\omega}_1 + \frac{1}{2} \boldsymbol{\omega}_2 \cdot \mathbf{I}_2 \cdot \boldsymbol{\omega}_2 + \frac{1}{2} \frac{M_1 M_2}{M_1 + M_2} \mathbf{v} \cdot \mathbf{v} + \mathcal{U}_{11} + \mathcal{U}_{22} + \mathcal{U}_{12} \quad (8)$$

where M_1 and M_2 are the masses of the two components, \mathbf{r} and \mathbf{v} are the relative position and velocity vector between these two components, \mathcal{U}_{ii} is the self-potential of the new components and \mathcal{U}_{12} is the mutual potential between the components.

$$\mathcal{U}_{12} = -G \int_{\beta_1} \int_{\beta_2} \frac{dm_1 dm_2}{|\boldsymbol{\rho}_1 - \boldsymbol{\rho}_2|} \quad (9)$$

The mutual potential represents a conduit for energy being transferred from rotational to translational energy and vice-versa and can be surprisingly effective.

Model of the proto-binary separation

- explains the observed correlation P_1 vs q

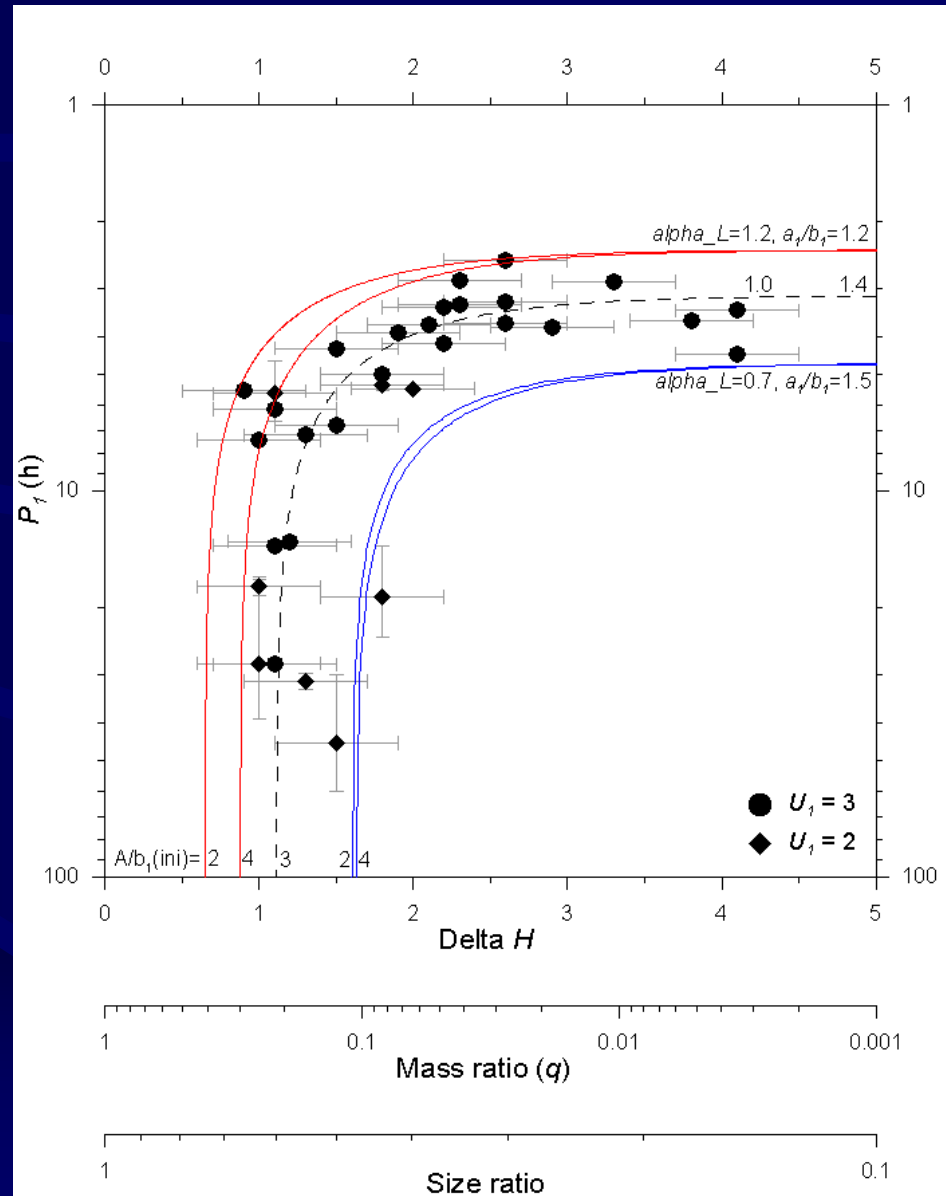
Model curves for following parameters:

- $\alpha_L = 0.7, 1.0, 1.2$
(total angular momentum near the lower, middle and upper values observed in orbiting binary systems)
- initial separations $A/b_1 = 2$ and 4
(orbit's semimajor axis/medium semiaxis of the primary)
- primary's equatorial axes ratio $a_1/b_1 = 1.2 - 1.5$ (from observed amplitudes).

Primaries of pairs with small mass ratios ($q = 10^{-3}$ to a few 10^{-2}) rotate rapidly near the critical fission frequency.

As the mass ratio approaches the approximate cutoff limit of 0.2, the primary period grows long, as when the total energy of the system approaches zero to disrupt the asteroid pair must extract an increasing fraction of the primary's spin energy.

Asteroid pairs were formed by rotational fission of critically spinning parent asteroids. (Pravec et al. 2010)



Yarkovsky-O'Keefe-Radzievskii-Paddack (YORP) effect

Changes asteroid spin vectors

- a key evolutionary process in small asteroids
(Task 5)

Yarkovsky-O'Keefe-Radzievskii-Paddack (YORP) effect

PLANETARY SCIENCE

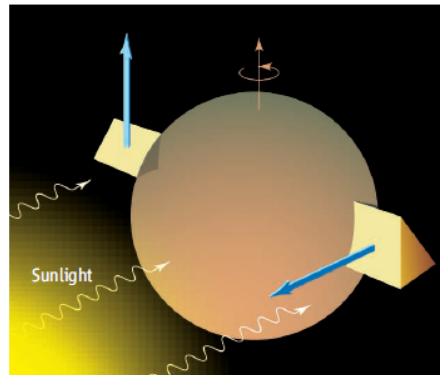
As Tiny Worlds Turn

David P. Rubincam and Stephen J. Paddack

Sunlight changes the rotation rate of an asteroid? The idea seems absurd, but on page 272 Lowry *et al.* (1) and on page 274 Taylor *et al.* (2) report observations that indicate sunlight is doing just that to the small asteroid 2000 PH5, and Kaasalainen *et al.* indicate the same is happening on 1862 Apollo (3). The mechanism is the Yarkovsky-O'Keefe-Radzievskii-Paddack effect, mercifully shortened to YORP. With YORP now on a solid foundation, we may be able to understand a number of strange observations involving small spinning asteroids and asteroid binary systems.

The saga of sunlight changing into spin began with Ivan Yarkovsky, a Polish engineer who realized more than a century ago that the infrared radiation escaping a body warmed by sunlight carries off momentum as well as heat (4). Point this heat in the right direction, and it will function like a rocket motor: Each infrared photon escaping the object carries away momentum, thanks to the relationship $p = E/c$, where p is the photon's momentum, E is its

The authors are with NASA Goddard Space Flight Center, Greenbelt, MD 20771, USA. E-mail: David.P.Rubincam@nasa.gov



Spinning in the Sun. Sunlight speeds up rotation due to reflection off the vertical and slanted faces of the wedges (blue arrows). Infrared radiation emitted by the faces also causes speed-up. If the body spins in the opposite sense, then YORP will slow it down.

energy, and c is the speed of light. By the principle of action-reaction, the object emitting the photon gets a kick in the opposite direction. (Yarkovsky knew nothing of photons and based his reasoning on the outmoded ether concept, but his idea survives the translation to modern physics.) Yarkovsky thrust is tiny, but space is

Rotational force produced by sunlight may help explain the movement of small asteroids, unusual asteroid orbits, and asteroid pairs.

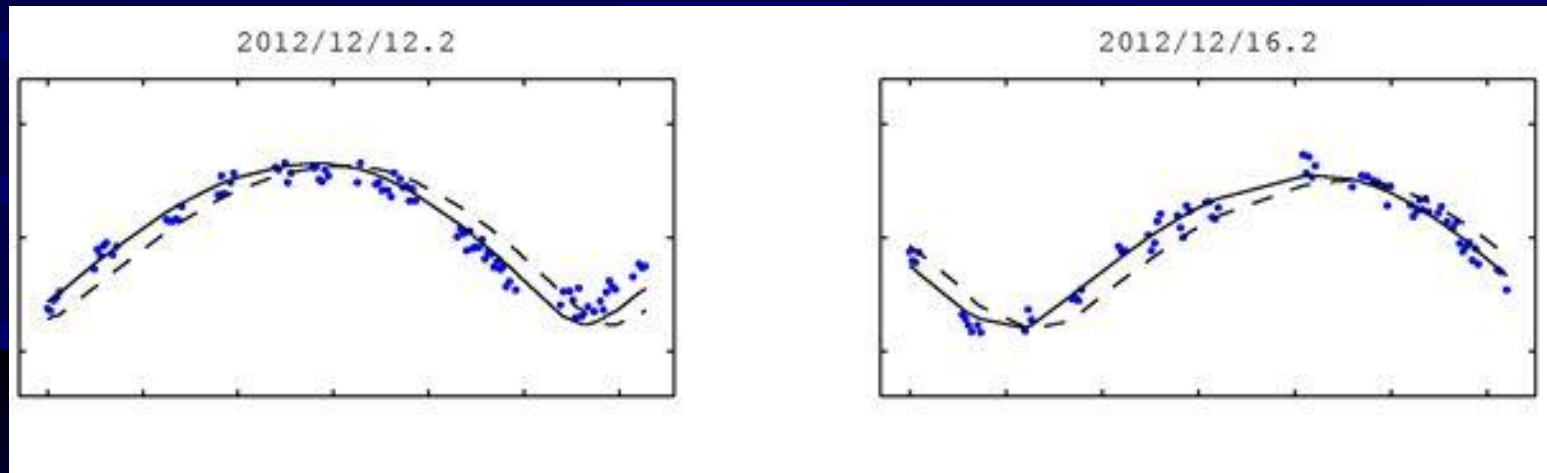
so empty there is no friction to stop it. Moreover, because the Sun is always shining, the Yarkovsky effect goes on century after century with an inexhaustible supply of photonic fuel, profoundly altering the orbits of meter-sized meteoroids (5).

V. V. Radzievskii applied the photon thrust idea to rotation by imagining each face of a cubical meteoroid painted white on one half and black on the other; sunlight reflected by the white part pushes that area more than the black half, causing a torque, which changes the rotation rate (6). His mechanism is weak because the black half, although it reflects little, makes up much of the difference by emitting infrared photons. Moreover, most small solar system objects have fairly uniform albedoes (that is, the fraction of light reflected) across their surfaces.

Building on this work, John A. O'Keefe and one of us (S.J.P.) at NASA realized that shape was a much more effective means of altering a body's spin rate than albedo and set about measuring spin changes in the laboratory. The idea was that light reflecting off of various angled surfaces on the object could

Yarkovsky-O'Keefe-Radzievskii-Paddack (YORP) effect

Fázový posun ve světelné křivce asteroidu (25143) Itokawa - projev YORPu



Non-principal axis rotators (“tumblers”) among the smallest asteroids

Asteroids in excited rotation states
(Task 7)

Force-free precession

Non-principal axis rotation (free precession, tumbling) is a spin state with higher than minimal rotational kinetic energy for given angular momentum L .

Appendix A: Force-free precession

Free precession has been well discussed by many authors (see, e.g., Samarasinha & A'Hearn 1991 and references therein). However, some subjects needed in the inverse problem require special attention, so I give a concise account of the dynamical problem here.

The time evolution of the Euler angles ϕ , θ , ψ is easy to derive from the basic kinematic equations (see, e.g., Goldstein 1980) that can be written as

$$\begin{aligned}\frac{L_1}{I_1} &= \dot{\phi} \sin \theta \sin \psi + \dot{\theta} \cos \psi, \\ \frac{L_2}{I_2} &= \dot{\phi} \sin \theta \cos \psi - \dot{\theta} \sin \psi, \\ \frac{L_3}{I_3} &= \dot{\phi} \cos \theta + \dot{\psi},\end{aligned}\quad (\text{A.1})$$

where L_i are the projections of the angular momentum vector \mathbf{L} onto the principal axes of the tumbling inertia ellipsoid; \mathbf{L} is constant in an inertial frame in torque-free precession. The components L_i are, by the definition of the Euler angles,

$$(L_1, L_2, L_3) = (L \sin \theta \sin \psi, L \sin \theta \cos \psi, L \cos \theta). \quad (\text{A.2})$$

Combining the two sets of equations, we get

$$\begin{aligned}\dot{\phi} &= L(I_+ - I_- \cos 2\psi), \\ \dot{\theta} &= L I_- \sin \theta \sin 2\psi,\end{aligned}\quad (\text{A.3})$$

$$\dot{\psi} = \cos \theta \left(\frac{L}{I_3} - \dot{\phi} \right),$$

where $I_+ = \frac{1}{2}(I_1^{-1} + I_2^{-1})$ and $I_- = \frac{1}{2}(I_1^{-1} - I_2^{-1})$. The basic properties of the time evolution of the Euler angles are quite apparent from this set of equations: when

The rotational motion can be described with the time evolution of the Euler angles (e.g., Samarasinha and A'Hearn 1991, Kaasalainen 2001).

It is a rotation around one of the extreme principal inertia axes and a precession of the axis around the L vector.

Two periods: P_ϕ , P_ψ

pensive function calls to each point separately. It is useful to evaluate one quantity via an elliptic integral; this is the rotation period P_ψ , given by

$$P_\psi = 4 \sqrt{\frac{I_1 I_2 I_3}{2E(I_1 - I_3)(I_2 - \frac{L^2}{2E})}} K(k), \quad (\text{A.7})$$

where $K(k)$ is the complete elliptic integral $K(k) = \int_0^{\pi/2} (\sqrt{1 - k^2 \sin^2 x})^{-1} dx$, and

$$k^2 = \frac{(I_2 - I_1) \left(\frac{L^2}{2E} - I_3 \right)}{(I_1 - I_3) \left(I_2 - \frac{L^2}{2E} \right)}. \quad (\text{A.8})$$

The rotational motion of an asteroid is described by

$$\vec{L} = \hat{I} \vec{\omega}, \quad (1)$$

where \vec{L} is the asteroid's angular momentum vector, \hat{I} is its inertia tensor, and $\vec{\omega}$ is its angular velocity vector. The inertia tensor is generally a symmetric tensor containing six independent components. A convenient choice of the system of coordinates in the asteroid-fixed frame gives zero non-diagonal components. The diagonal components $I_1 \leq I_2 \leq I_3$ are then the principal moments of inertia; the axes are called the principal inertia axes.

The rotational kinetic energy is generally

$$E = \frac{1}{2} \vec{\omega}^T \hat{I} \vec{\omega} \quad (2)$$

and particularly for the principal inertia axes choice of the system of coordinates

$$E = \frac{1}{2} (I_1 \omega_1^2 + I_2 \omega_2^2 + I_3 \omega_3^2). \quad (3)$$

(Pravec et al. 2005)

(Kaasalainen 2001)

Using the constant

$$\Delta\phi = \int_0^{P_\psi} \dot{\phi} dt = 2 \int_0^{P_\psi/2} \dot{\phi} dt \quad (\text{A.10})$$

(note that $\Delta\phi$ is independent of L , whose occurrences in P_ψ and $\dot{\phi}$ cancel each other out), we can define

$$P_\phi = 2\pi \frac{P_\psi}{\Delta\phi}. \quad (\text{A.11})$$

Tumbler lightcurve

Lightcurve of a tumbling asteroid can be expanded with the Fourier series in the two angular variables (Kaasalainen 2001, Pravec et al. 2005).

In a tumbler's lightcurve, we observe the frequencies $f_\varphi = P_\varphi^{-1}$, $f_\psi = P_\psi^{-1}$, and their linear combinations.

The highest signal is often observed in the second harmonic of ($f_\varphi \pm f_\psi$); it is the actual mean frequency of rotation of the body around the instantaneous spin axis.

Appendix A. Fourier series in two dimensions

A function $F(\psi, \phi)$, where ψ, ϕ are angular variables over $(-\pi, \pi)$, can be expanded with Fourier series in the two variables (Rektorys et al., 1988):

$$F(\psi, \phi) = \sum_{j,k=0}^{\infty} [a_{jk} \cos j\psi \cos k\phi + b_{jk} \sin j\psi \cos k\phi + c_{jk} \cos j\psi \sin k\phi + d_{jk} \sin j\psi \sin k\phi], \quad (\text{A.1})$$

where

$$a_{jk} = \frac{\lambda_{jk}}{\pi^2} \int_{-\pi}^{\pi} \int_{-\pi}^{\pi} F(\psi, \phi) \cos j\psi \cos k\phi \, d\psi \, d\phi, \quad (\text{A.2})$$

$$b_{jk} = \frac{\lambda_{jk}}{\pi^2} \int_{-\pi}^{\pi} \int_{-\pi}^{\pi} F(\psi, \phi) \sin j\psi \cos k\phi \, d\psi \, d\phi, \quad (\text{A.3})$$

$$c_{jk} = \frac{\lambda_{jk}}{\pi^2} \int_{-\pi}^{\pi} \int_{-\pi}^{\pi} F(\psi, \phi) \cos j\psi \sin k\phi \, d\psi \, d\phi, \quad (\text{A.4})$$

(Pravec et al. 2005)

$$d_{jk} = \frac{\lambda_{jk}}{\pi^2} \int_{-\pi}^{\pi} \int_{-\pi}^{\pi} F(\psi, \phi) \sin j\psi \sin k\phi \, d\psi \, d\phi, \quad (\text{A.5})$$

$$\lambda_{jk} = \left(\frac{1}{2}\right)^{\delta_j^0} \left(\frac{1}{2}\right)^{\delta_k^0}, \quad (\text{A.6})$$

and δ_i^0 is Kronecker's delta.

The Fourier series given by Eq. (A.1) can be rewritten into a following form that is convenient for some purposes:

$$F(\psi, \phi) = C_0 + \sum_{j=1}^{\infty} [C_{j0} \cos j\psi + S_{j0} \sin j\psi] + \sum_{k=1}^{\infty} \sum_{j=-\infty}^{\infty} [C_{jk} \cos(j\psi + k\phi) + S_{jk} \sin(j\psi + k\phi)], \quad (\text{A.7})$$

where

$$\begin{aligned} C_0 &= a_{00}, & C_{j0} &= a_{j0}, & S_{j0} &= b_{j0}, \\ C_{0k} &= a_{0k}, & S_{0k} &= c_{0k}, \\ C_{\pm j,k} &= \frac{a_{jk} \pm d_{jk}}{2}, & S_{\pm j,k} &= \frac{c_{jk} \pm b_{jk}}{2}, \end{aligned} \quad (\text{A.8})$$

for $j, k > 0$.

Lightcurve of a fast spinning tumbler (2002 TD60)

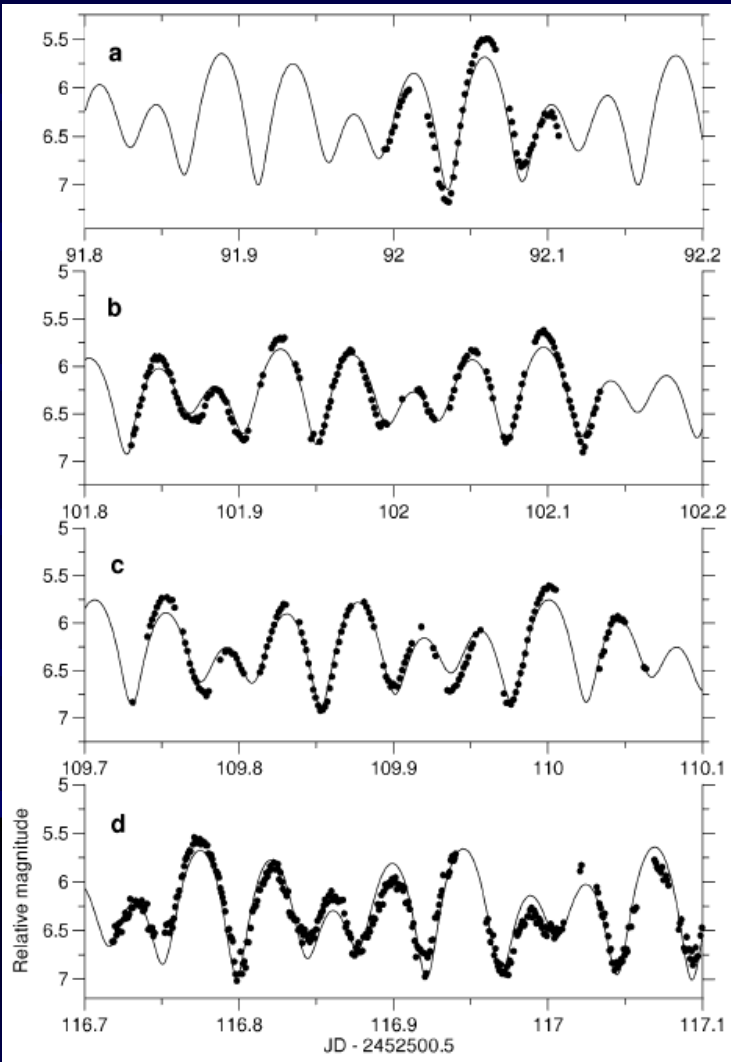


Fig. 4. Lightcurve data of 2002 TD₆₀ of (a) 2002-11-14.1, (b) 11-24.0, (c) 12-01.9, and (d) 12-08.9, respectively. Curve is the best-fit synthetic lightcurve of the prograde solution of the numerical model. The other, mirror solution (retrograde) gives a curve indistinguishable from the plotted one.

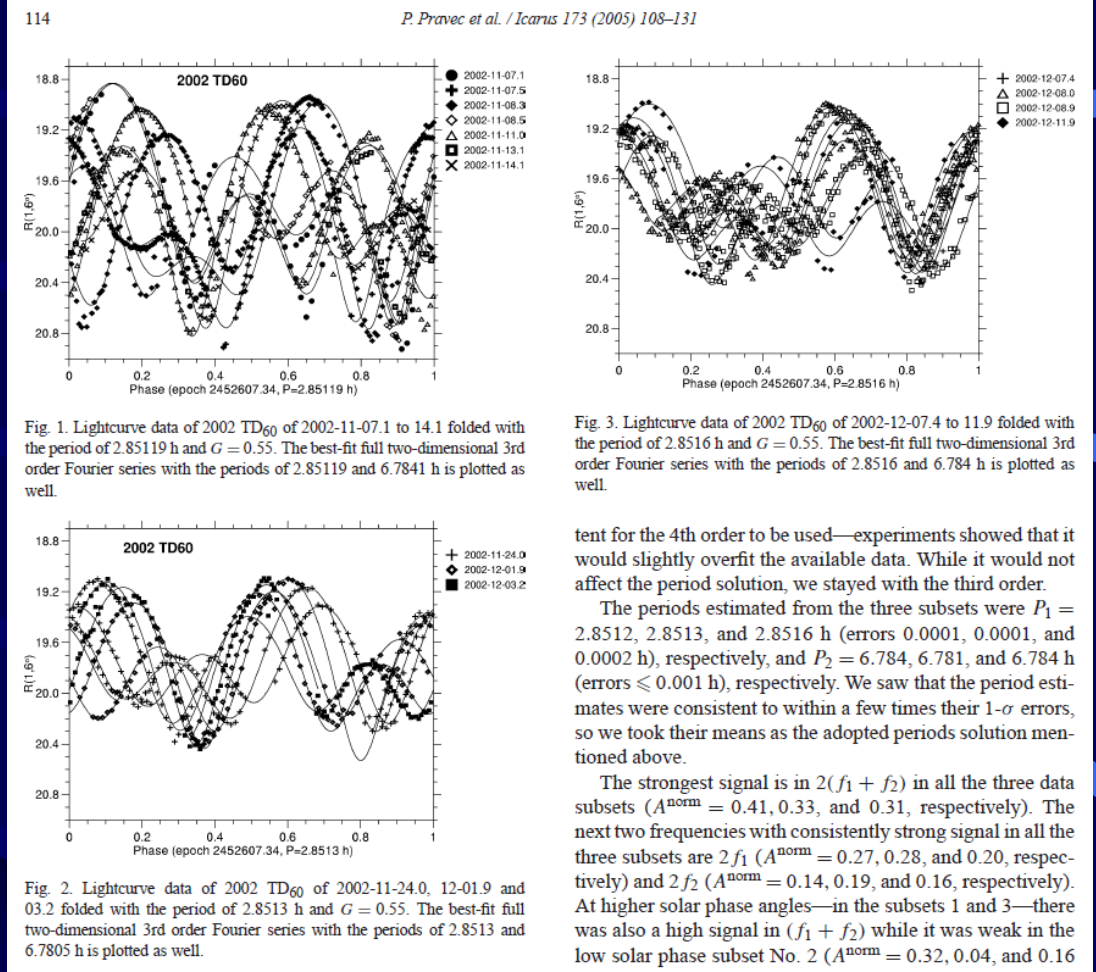


Fig. 1. Lightcurve data of 2002 TD₆₀ of 2002-11-07.1 to 14.1 folded with the period of 2.85119 h and $G = 0.55$. The best-fit full two-dimensional 3rd order Fourier series with the periods of 2.85119 and 6.7841 h is plotted as well.

Fig. 2. Lightcurve data of 2002 TD₆₀ of 2002-11-24.0, 12-01.9 and 03.2 folded with the period of 2.8513 h and $G = 0.55$. The best-fit full two-dimensional 3rd order Fourier series with the periods of 2.8513 and 6.7805 h is plotted as well.

Fig. 3. Lightcurve data of 2002 TD₆₀ of 2002-12-07.4 to 11.9 folded with the period of 2.8516 h and $G = 0.55$. The best-fit full two-dimensional 3rd order Fourier series with the periods of 2.8516 and 6.784 h is plotted as well.

tent for the 4th order to be used—experiments showed that it would slightly overfit the available data. While it would not affect the period solution, we stayed with the third order.

The periods estimated from the three subsets were $P_1 = 2.8512, 2.8513, \text{ and } 2.8516 \text{ h}$ (errors 0.0001, 0.0001, and 0.0002 h), respectively, and $P_2 = 6.784, 6.781, \text{ and } 6.784 \text{ h}$ (errors $\leq 0.001 \text{ h}$), respectively. We saw that the period estimates were consistent to within a few times their $1-\sigma$ errors, so we took their means as the adopted periods solution mentioned above.

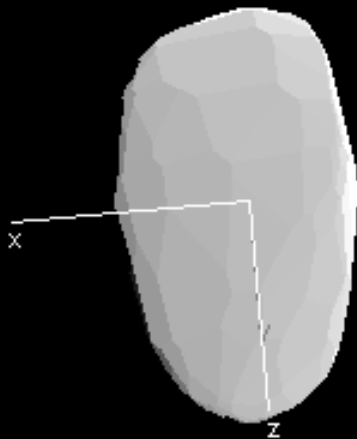
The strongest signal is in $2(f_1 + f_2)$ in all the three data subsets ($A^{\text{norm}} = 0.41, 0.33, \text{ and } 0.31$, respectively). The next two frequencies with consistently strong signal in all the three subsets are $2f_1$ ($A^{\text{norm}} = 0.27, 0.28, \text{ and } 0.20$, respectively) and $2f_2$ ($A^{\text{norm}} = 0.14, 0.19, \text{ and } 0.16$, respectively). At higher solar phase angles—in the subsets 1 and 3—there was also a high signal in $(f_1 + f_2)$ while it was weak in the low solar phase subset No. 2 ($A^{\text{norm}} = 0.32, 0.04, \text{ and } 0.16$

2008 TC3 numerical model

- Best-fit shape:

2008 TC3
JD=2454746.491705 (2008/10/06 23:48:03)

$\phi = 112.7$
 $\theta = 61.9$
 $\psi = 77.8$



Dimensions ratio:

$$z/x = 2.4$$

$$y/x = 1.3$$

The shape is convex model only!

(Scheirich et al. 2010)

(99942) Apophis

A 400-meter asteroid with a small but non-zero Earth impact probability (several possible impact dates in the 21st century; Farnocchia et al., 2013).

The most significant uncertainty in the prediction - an unknown magnitude and sign of the Yarkovsky drift of the Apophis' orbit.

The Yarkovsky drift depends on asteroid's spin state, angular momentum vector, and size.

Little was known about its spin before; limited data by Behrend et al. suggested a slow rotation with a period about 30 hours.

Our analysis of their data indicated a possibility that it might be tumbling.

We undertook the task of establishing its spin state within our NEOSource project.

Photometry of Apophis

Apparition: 2012 Dec. 23 – 2013 April 15

Data from
35 nights with the 1.54-m Danish telescope, La Silla



topography especially in lightcurve minima \rightarrow am

Apophis' tumbling

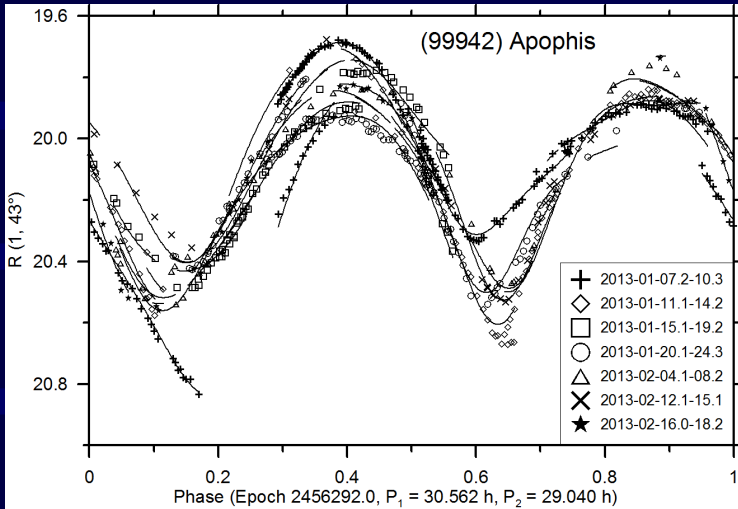


Table 2

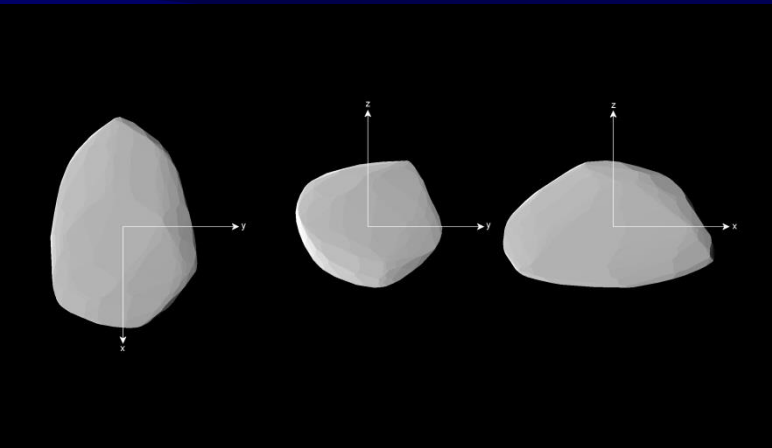
Parameters of the Apophis model with their estimated admissible uncertainties (corresponding to 3σ confidence level).

Fitted parameters	
λ_L ($^\circ$)	250 ^a
β_L ($^\circ$)	-75
ϕ_0 ($^\circ$)	152 ⁺¹⁷³ ₋₆₄
ψ_0 ($^\circ$)	14 ⁺⁴⁴ ₋₁₁
P_ψ (h)	263 ± 6
P_ϕ (h)	27.38 ± 0.07
$I_a \equiv I_1/I_3$	0.61 ^{+0.11} _{-0.08}
$I_b \equiv I_2/I_3$	0.965 ^{+0.009} _{-0.015}
Derived parameters	
$(P_\phi^{-1} - P_\psi^{-1})^{-1} = P_1$ (h)	30.56 ± 0.01
θ_{\min} ($^\circ$)	12 ± 4
θ_{\max} ($^\circ$)	55 ⁺⁹ ₋₂₀
θ_{aver} ($^\circ$)	37 ⁺⁶ ₋₁₄
$a_{\text{dyn}}/c_{\text{dyn}}$	1.51 ± 0.18
$b_{\text{dyn}}/c_{\text{dyn}}$	1.06 ± 0.02
$a_{\text{shp}}/c_{\text{shp}}$	1.64 ± 0.09
$b_{\text{shp}}/c_{\text{shp}}$	1.14 ^{+0.04} _{-0.08}
E/E_0	1.024 ± 0.013

The angles ϕ_0 and ψ_0 are for the epoch JD 2456284.676388 (=2012 December 23.176388 UT), light-travel time corrected (i.e., astero-centric).

E/E_0 is a ratio of the rotational kinetic energy and the lowest energy for given angular momentum, defined as $E_0 = L^2/(2I_3)$.

^a The major and minor semiaxes of the uncertainty area of the direction of \vec{L} are 27° and 14°, respectively, see Fig. 4.



For the Apophis' spin state, the impact on 2068 April 12 is possible. Its probability is still low, on an order of 10^{-5} , but it requires more study, observations and modeling.

Conclusions

The Danish 1.54-m telescope is a small but very good dedicated photometric telescope.

It is a great instrument for observations requiring long time series.

Taking them is possible for the combination of the capabilities of the telescope system allowing inexpensive remote observations, the exceptional quality of the sky on La Silla, and the collaborative spirit of the people running the telescope (the Danish team, the Czech team, and the ESO La Silla staff).

We are getting unique data and results on properties and processes in near-Earth asteroids in particular.